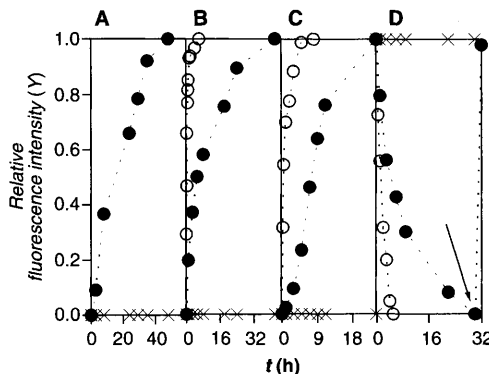


Fig. 3. Real-time enzyme screening with (A) apyrase, (B) aldolase, (C) alkaline phosphatase, and (D) galactosyltransferase without and (arrow) with CIAP, using **2**. Fractional pore activity γ (18) after addition of 20 μ l of reaction mixture and **2** to LUVs \supset CF is shown as a function of reaction time. Reaction mixtures: (A) 0 (\times) and 4 (\bullet) U/ml apyrase, 40 mM ATP; (B) 0 (\times), 2 (\bullet), and 16 (\circ) U/ml RAMA, 750 U/ml triosephosphate isomerase (TIM), 40 mM D-fructose 1,6-diphosphate (FDP); (C) 0 (\times), 66 (\bullet), and 670 (\circ) U/ml CIAP, 800 mM UDP; (D) 0 (\times), 8 (\bullet , arrow: addition of 66 U/ml CIAP), and 32 (\circ) U/ml galactosyltransferase, 250 mM *N*-acetylglucosamine (GlcNAc), 375 mM UDPGal [or 375 mM NAcUDPGal (20)] (18).



pore **2** (Fig. 1) (18). As expected from specific guanidinium-phosphate interactions (19), $K_D^{\text{min}} = 2 \mu\text{M}$ determined for ATP demonstrated increased sensitivity (by a factor of >1000) of apyrase sensor **2** compared to **1** \supset Mg^{2+} (17, 18).

The most important adaptability of pore **2** to sense various enzymes was exemplified with real-time detection of selected classes of enzymes for which noninvasive assays compatible with high-throughput substrate screening for the development of enzymatic carbohydrate and oligosaccharide synthesis (10–12) are needed. As with apyrase, rabbit muscle aldolase (RAMA) (10) and calf intestine alkaline phosphatase (CIAP) (11) converted strong channel blockers into poor ones (Table 1, entries 5 to 7). Enzyme-catalyzed substrate consumption was thus reported by the decreasing ability of the reaction mixture to hinder CF efflux through **2** with increasing reaction time, i.e., “enzyme-gated” pore formation (Fig. 3, A to C). Bovine milk galactosyltransferase (11, 12), in contrast, produced uridine diphosphate (UDP) with $K_D^{\text{min}} = 1.2 \text{ mM}$ from two poor blockers (Table 1, entry 8). This enzyme was therefore detectable by decreasing activity of pore **2** with increasing reaction time (Fig. 3D). Use of CIAP to eliminate UDP blockage (Fig. 3D, arrow) corroborated the proposed mechanism and demonstrated the possibility to detect two enzymes simultaneously or, from a different point of view, to turn synthetic multifunctional pores “off” and “on” using enzymes only.

Taken together, these results demonstrate practical usefulness of synthetic supramolecular pores for fluorometric detection of enzyme activity, a topic of current scientific interest (13). The most important characteristic of our assay is adaptability of the same supramolecular sensor to a broad variety of substrates and enzymes. There is no need to prepare new, substrate- or product-specific antibodies [as for catalytic assays using enzyme-linked immunosorbent assay (cat-ELISA) and related assays] or synthetic receptors for individual enzymes; no need to label substrates as in fluorogenic and radio-

assays; and no need to calibrate coupled multienzyme assays (13, 14). Whereas intrinsic limitations concerning, e.g., hydrophobic or lytic substrates, certain more complex analytes (18), continuous assay, or in vivo detection will be challenging to overcome, at least in a general manner, there is much room to implement various in vitro formats compatible with high-throughput screening and miniaturization (1).

References and Notes

1. H. Bayley, P. S. Cremer, *Nature* **413**, 226 (2001).
2. S. Cheley, L. Gu, H. Bayley, *Chem. Biol.* **9**, 829 (2002).
3. P. Scrimin, P. Tecilla, *Curr. Opin. Chem. Biol.* **3**, 730 (1999).
4. G. W. Gokel, A. Mukhopadhyay, *Chem. Soc. Rev.* **30**, 274 (2001).

5. G. J. Kirkovits, C. D. Hall, *Adv. Supramol. Chem.* **7**, 1 (2000).
6. S. Matile, *Chem. Soc. Rev.* **30**, 158 (2001).
7. G. Das, S. Matile, *Proc. Natl. Acad. Sci. U.S.A.* **99**, 5183 (2002).
8. G. Das, H. Onouchi, E. Yashima, N. Sakai, S. Matile, *ChemBioChem* **3**, 1089 (2002).
9. Without high-resolution crystallographic evidence, it is not incorrect to perceive the depicted suprastructures as, at worst, productive working hypotheses that are consistent with all (6–8) functions discovered so far.
10. T. D. Machajewski, C.-H. Wong, *Angew. Chem. Int. Ed.* **39**, 1352 (2000).
11. M. M. Palcic, *Methods Enzymol.* **230**, 300 (1994).
12. N. Wymer, E. J. Toone, *Curr. Opin. Chem. Biol.* **4**, 110 (2000).
13. D. Wahler, J.-L. Reymond, *Curr. Opin. Chem. Biol.* **5**, 152 (2001).
14. A. W. Czarnik, *Acc. Chem. Res.* **27**, 302 (1994).
15. M. Komoszynski, A. Wojtczak, *Biochim. Biophys. Acta* **1310**, 233 (1996).
16. G. M. Whitesides et al., *Acc. Chem. Res.* **28**, 37 (1995).
17. All reported K_D values are conditional to the method (Hill analysis of concentration dependence) specified in (8).
18. See supporting data on Science Online.
19. T. S. Snowden, E. V. Anslyn, *Curr. Opin. Chem. Biol.* **3**, 740 (1999).
20. G. Das, P. Talukdar, S. Matile, data not shown.
21. We thank J.-L. Reymond and N. Sakai for advice, J. Gruenberg for access to still video camera and fluorescence counter, and the Swiss NSF (2000-064818.01 and National Research Program “Supramolecular Functional Materials” 4047-057496) for financial support.

Supporting Online Material

www.sciencemag.org/cgi/content/full/298/5598/1600/DC1
Materials and Methods
References and Notes

14 August 2002; accepted 14 October 2002

Arsenic Mobility and Groundwater Extraction in Bangladesh

Charles F. Harvey,¹ Christopher H. Swartz,^{1*}
A. B. M. Badruzzaman,² Nicole Keon-Blute,¹ Winston Yu,¹
M. Ashraf Ali,² Jenny Jay,¹ Roger Beckie,³ Volker Niedan,¹
Daniel Brabander,^{1†} Peter M. Oates,¹ Khandaker N. Ashfaque,¹
Shafiqul Islam,⁴ Harold F. Hemond,¹ M. Feroze Ahmed²

High levels of arsenic in well water are causing widespread poisoning in Bangladesh. In a typical aquifer in southern Bangladesh, chemical data imply that arsenic mobilization is associated with recent inflow of carbon. High concentrations of radiocarbon-young methane indicate that young carbon has driven recent biogeochemical processes, and irrigation pumping is sufficient to have drawn water to the depth where dissolved arsenic is at a maximum. The results of field injection of molasses, nitrate, and low-arsenic water show that organic carbon or its degradation products may quickly mobilize arsenic, oxidants may lower arsenic concentrations, and sorption of arsenic is limited by saturation of aquifer materials.

In an effort to prevent waterborne disease, Bangladesh shifted its drinking water supply from surface to groundwater. Many of the

recently installed 6 to 10 million drinking-water wells contain high concentrations of arsenic (1), causing widespread arsenicosis

and threatening to increase cancer rates (2). Sediments typically contain only modest levels of arsenic (1), and the cause and timing of arsenic mobilization from these sediments remain unclear (3). Some have argued that arsenic is mobilized by slow reduction of iron oxyhydroxides or sorbed arsenate by detrital organic carbon (1, 4, 5). Others have suggested that arsenic may have recently been released through sulfide oxidation reactions induced by the massive increase in dry-season irrigation pumping (6, 7). Here, we characterize aqueous and solid phases at one site to show that young carbon brought to depth by recent irrigation pumping plays a role in mobilization.

Our study site was located in the Munshiganj district, 30 km south of Dhaka and 7 km north of the Ganges River. We installed 17

sampling wells within 5 m of each other to depths from 5 to 165 m, sampled 54 monitoring wells in a 16-km² region, and collected three sediment cores [e.g., (8)]. The site is typical of southern Bangladesh (9) and includes 3 m of surficial clay, a 100-m aquifer of gray sand (Holocene aquifer), a 40-m aquitard of marine clay, and a deep burnt-orange sandy aquifer (Pleistocene aquifer). The aquifers are ~85% quartz and feldspar by weight, with the remainder composed of biotite, hornblende, magnetite, and a variety of other minerals. We found no peat, which has been hypothesized to be associated with dissolved As (10). The pH of the groundwater was 6.6 (4.6 m) to 7.1 (107 m) in the upper aquifer, and 6.8 in the lower aquifer (165 m). In both aquifers, redox measurements by platinum electrode are between 20 and 90 mV (corrected to the standard hydrogen electrode), and only one depth (14 m) has a dissolved O₂ concentration (0.33 mg/liter) greater than 0.2 mg/liter (our approximate limit of detection).

Dissolved As concentrations (>90% As(III)) peaked at a depth of 30 to 40 m (Fig. 1A). Solid-phase As exceeded 27 nmol/g (2 ppm) in only one sample from the sandy aquifers and never exceeded 100 nmol/g (8 ppm) in the clays. Solid-phase As (Fig. 1B) is adsorbed, coprecipitated in solids leachable by mild acids and reductants, incorporated in silicates, and incorporated in solids that are

dissolved only by cold and hot nitric acid (most likely crystalline sulfides) [e.g., (8, 11)]. The distribution of arsenic among these pools is similar throughout the deep and shallow sediments, with no apparent correspondence to the peak in dissolved As.

The inverse relation of dissolved sulfate with arsenic (Fig. 1C) in the natural groundwater, and the presence of acid volatile sulfide (AVS) in the sediments near the dissolved As peak, suggest that oxidative dissolution of pyrite has not liberated arsenic. Instead, low dissolved sulfur levels appear to limit the precipitation of arsenic sulfides near the arsenic peak. To test whether oxidants may mobilize arsenic, we injected nitrate into the aquifer. Dissolved As levels declined (Fig. 2A), probably as a result of adsorption on iron oxyhydroxides precipitated by a microbial process such as described in (12). Arsenic concentrations remained low even after the volume extracted exceeded the volume injected, perhaps indicating arsenic removal in a geochemically altered zone of increased sorption capacity around the injection well.

Solid-phase As and Fe appear to be associated. Arsenic (Fig. 1B) and iron released from sediments in the first five extractants in a sequential extraction procedure are correlated ($r^2 = 0.64$) among samples from different depths, although dissolved Fe(II) (ranging

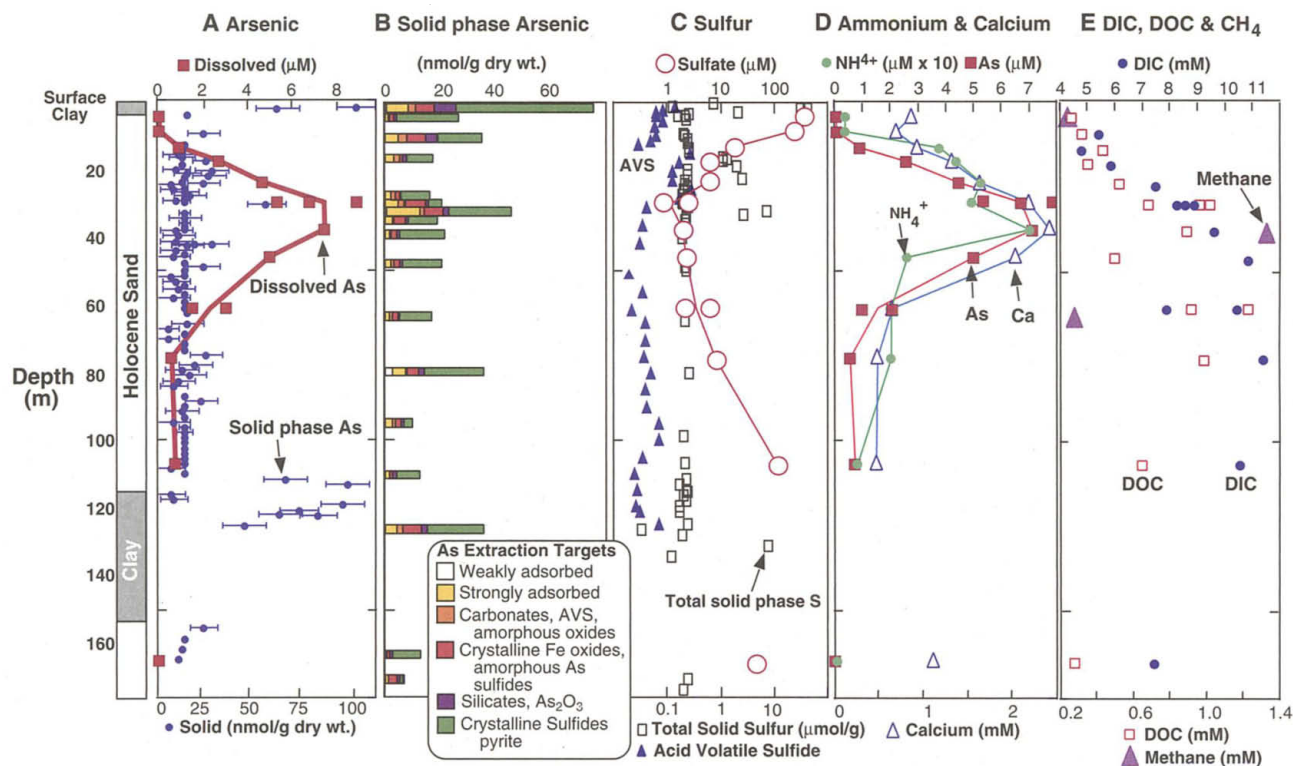
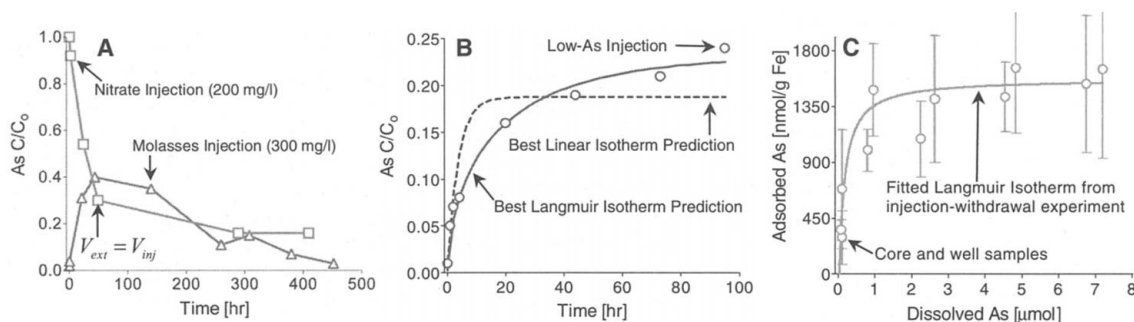


Fig. 1. Vertical profiles of subsurface geochemical characteristics in Munshiganj. (A) Dissolved As levels peak at 8.5 μM or 640 ppb, well above the Bangladeshi standard of 50 ppb. (B) Arsenic dissolved by the sequence of extractions that target different solid phases [e.g., (8, 17)]. (C) Dissolved As and sulfate are inversely related. (D) Dissolved As, ammonium, and calcium are closely correlated. (E) DIC, DOC, and methane increase with depth to 31 m.

Fig. 2. Arsenic levels responded within hours after chemical perturbations in three injection-withdrawal experiments: (i) nitrate, 500 liters from the 38-m well [$7.2 \mu\text{M}$ As, with nitrate (200 mg/liter) added] into a 31-m well (concentration at the well before injection $C_0 = 6.5 \mu\text{M}$); (ii) molasses, 8000 liters from the 160-m well [$<0.01 \mu\text{M}$ As, with molasses (300 mg/liter) added] into a 105-m well ($C_0 = 0.8 \mu\text{M}$ As) filling $\sim 40 \text{ m}^3$ of aquifer material; and (iii) low-As water, 6052 liters of clean water from the 160-m well ($<0.01 \mu\text{M}$ As) into a 31-m well ($C_0 = 8.5 \mu\text{M}$ As). All injections included bromide (100 mg/liter) as tracer. (A) Arsenic concentrations (normalized by C_0) in withdrawn water after nitrate and molasses injections. (B) The arsenic rebound after injection of low-As water is well fit by a Langmuir isotherm, but not by a linear isotherm that does not represent limited

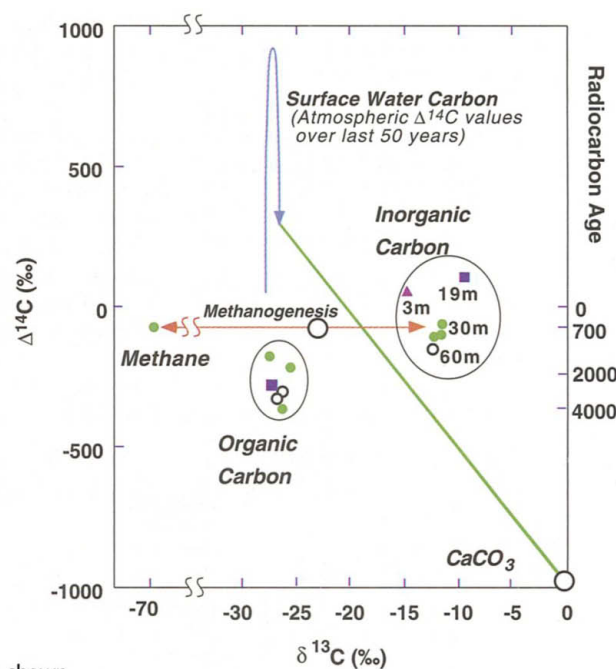


surface sites [e.g. (8)]. (C) The shape of the Langmuir isotherm is confirmed by the load of sorbed arsenic from core samples (shown in Fig. 1B) normalized by the easily extracted (HCl and oxalate) Fe and plotted against the dissolved As (Fig. 1A) for each depth. Error bars represent standard deviations of at least three samples from the 3-m well screen interval for each depth. The sorbed As predicted by the Langmuir model is normalized by 0.6 wt % Fe, the approximate value from core samples.

from 27 to $180 \mu\text{M}$) and solid-phase Fe (ranging from 1 to 3 wt % in the upper aquifer and 1 wt % in the lower aquifer) have no apparent systematic depth dependence. The sediment contains little, if any, purely ferric [Fe(III)] oxyhydroxides, which have been hypothesized to sequester and release arsenic (1, 4). Extraction results show that 60% of total solid-phase Fe was bound in silicates and pyritic phases, relatively immobile pools in anoxic water. The 10% of total iron extractable by 1 M HCl, which targets amorphous iron oxides, carbonates, and phosphates, was ferrous [Fe(II)] iron, as determined with ferrozine. Oxalic acid extraction, which targets amorphous iron oxyhydroxides and magnetite, and Ti(III)-citrate-EDTA extraction, which reductively dissolves iron oxides (and perhaps forms complexes with amorphous sulfides), each released 6% of total iron. Most of the iron in these pools can be explained as magnetite (a mixed-valence phase), which was measured by magnetic separation. Thus, if ferric oxyhydroxides control arsenic mobility, they do so in small quantities.

Surface sorption sites appeared to be saturated with arsenic where dissolved concentrations were high. Measured dissolved As concentrations from a field test, where water was withdrawn after injecting low-As groundwater into a high-As depth (Fig. 2B), were closely fit by a model that incorporates a Langmuir isotherm describing saturation of surface sites, but not by a linear isotherm [e.g. (8)]. The fitted Langmuir isotherm agrees remarkably well with dissolved and sorbed As concentrations measured at different depths (Fig. 2C). These results suggest that sorption sites saturate when dissolved As concentrations exceed 100 ppb; the implication is that when aqueous concentrations are high, little additional arsenic can be sorbed. Further arsenic inputs would likely be manifest as increased dissolved concentrations that are readily transported by flowing groundwater. High concentrations of phos-

Fig. 3. Carbon isotope values from groundwater samples. The $\Delta^{14}\text{C}$ ratios have been corrected for fractionation with the $\delta^{13}\text{C}$ ratios from the same samples. The circle on the orange line indicates the weighted average of methane (38 m depth) and DIC (31 m) isotope values, representing the isotopic values that DIC would have had before fractionation during carbonate reduction. The green line represents mixing between young terrestrial organic carbon (changing values due to bomb testing are shown by the rising and falling arrow) and geologic carbonate, which is found in the sediments. Because the inflowing DIC likely mixes with some old DIC, the radiocarbon date shown on the right axis may overestimate the age of the inflowing carbon. Symbols correspond to aquifer depth, as shown.



phate and silicate ($\sim 50 \mu\text{M}$ and $\sim 700 \mu\text{M}$, respectively, and nearly uniform with depth) as well as carbonate may contribute to the limited capacity to sorb arsenic oxyanions (13, 14). Iron phosphates and amorphous silica were both calculated to be supersaturated from measured aqueous concentrations, and we observed these phases by scanning electron microscopy as rims on host grains.

Ambient geochemical concentrations and the results of a field redox manipulation experiment both suggest that respiration of organic carbon plays a role in arsenic mobilization. Mobilization may be driven by reduction with organic carbon despite the paucity of ferric oxyhydroxides: Equilibrium chemical modeling indicates the dissolved As could have been sorbed by ferric oxyhydroxides in quantities of less than 5% of the iron liberated by oxalic acid.

Mobilization may also occur by displacement of arsenic by carbonate, a process recently proposed for ferric oxyhydroxides (13). Either process, or a combination, is consistent with the observed geochemical profiles. Dissolved NH_4^+ and Ca^{2+} profiles follow the dissolved As profile remarkably closely throughout the shallow aquifer (Fig. 1D), and dissolved organic and inorganic carbon (DOC and DIC) increase with increasing arsenic to the peak depth (Fig. 1E). The correlation between NH_4^+ and Ca^{2+} may be explained by respiration of DOC producing ammonia and CO_2 , with the latter inducing calcite dissolution. The molar ratio of carbonate to ammonium was ~ 70 (50 after subtracting carbonate liberated from calcite, assuming a 1:1 molar ratio of calcite carbonate to dissolved calcium), within the range for terrestrial organic material.

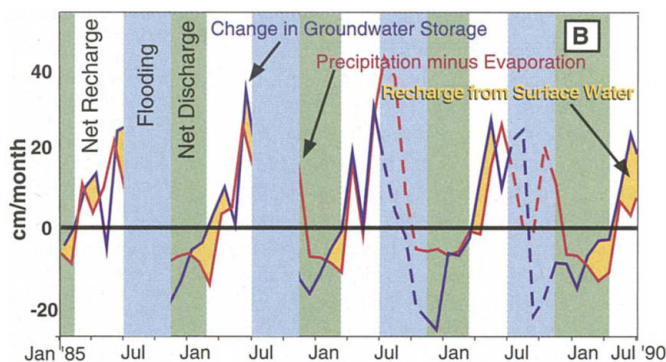
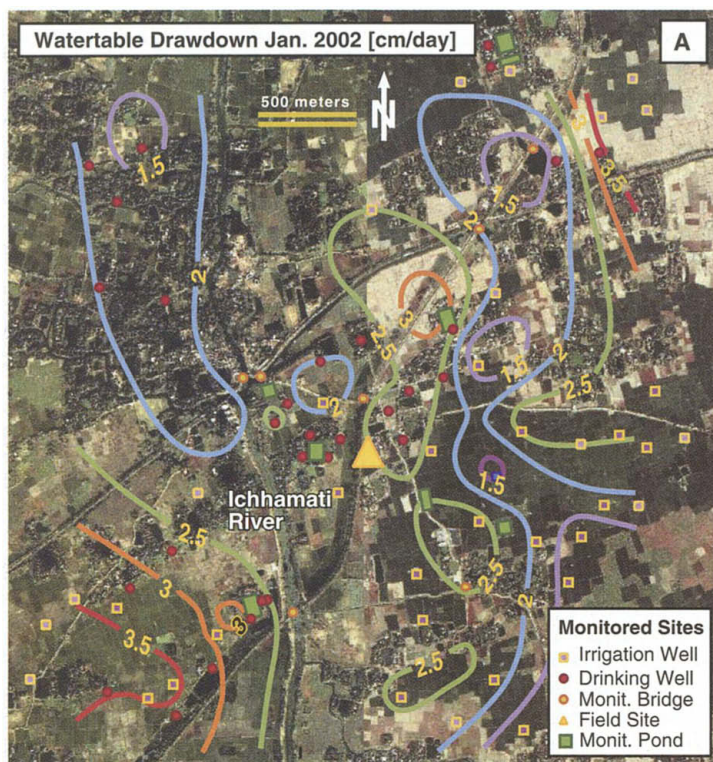


Fig. 4. (A) Water table drawdown contoured on an IKONOS satellite image with well positions. (B) Groundwater storage changes (draw-down times porosity) and net atmospheric recharge (rainfall minus evapotranspiration) determined from meteorological data. The difference between the change in storage (blue line) and the net atmospheric recharge (red line) is attributed to exchange with surface water. Surface water entered the aquifer when the change in groundwater storage was greater than net atmospheric recharge (shown in yellow). Inflow is evident during periods of water table decline (green strips) that typically occur from November to April, as well as during periods of water table rise (white strips), typically from April to June. During flooding (blue strips), the recorded hydraulic heads represent flood stage rather than changes in groundwater storage.

Field injection of molasses-amended groundwater produced an initial rise in arsenic concentration (Fig. 2A) concurrent with drops in platinum electrode readings (100 to -230 mV) and pH (6.7 to 5.6), followed by a drop in arsenic concentrations. Dissolved sulfate, which was introduced from the molasses, also fell (from ~ 300 μM to < 5 μM). These chemical changes are consistent with a scenario where the introduction of labile organic carbon caused microbially mediated dissolution of iron solids and liberation of arsenic, followed by precipitation of sulfides that sequestered arsenic.

As a further test, we analyzed carbon isotopes of groundwater. The radiocarbon ages for DOC are 3000 to 5000 years, consistent with wood fragments found at similar depths in nearby sediment (15). However, the radiocarbon ages for DIC in the same water samples are much younger, about 700 years at 31 m depth (Fig. 3), and ^{14}C is at bomb levels at 19 m, indicating carbon younger than 50 years. Because the young DIC cannot be the oxidative product of the older DOC, the presence of young DIC and old DOC in the same water samples must be explained either by mixing of invading younger water with older resident water, or by mobilization of older organic carbon from aquifer sediment into invading younger water. The similar profiles of DIC and DOC (Fig. 1E) are inconsistent with pore water mixing, which would create a negative correlation—recently recharged water would contain predominantly young carbon, whereas old resident water would

contain predominantly old carbon. The correlation instead is consistent with mobilization of old carbon through geochemical perturbations caused by the invasion of young water transporting young carbon, perhaps by release from iron oxyhydroxides, which are known to sequester organic carbon (16).

Methane concentrations reached 1.3 mM at 38 m (sufficient to effervesce flammable gas) and have approximately the same radiocarbon age as the DIC (Fig. 3). Because methane is an end product of carbon metabolism under anoxic conditions, recent biogeochemical reactions appear to have been driven by relatively young carbon carried by recent inflow of groundwater. The deuterium ratio of the methane ($\delta\text{D} = 197\text{‰}$) is consistent with fractionation during methanogenesis by carbonate reduction (17). The similar radiocarbon ages of methane and DIC also suggest that the methane was derived from the DIC pool. Ongoing carbonate reduction is consistent with high levels of dissolved hydrogen (10 nM at 38 m). Finally, the $\delta^{13}\text{C}$ values of both methane and DIC can be explained by fractionation during carbonate reduction. The weighted mean $\delta^{13}\text{C}$ value from methane at 38 m and carbonate at 31 m is -25‰ , a reasonable value for terrestrial carbon. Dissolution of radiocarbon-dead solid carbonate, as we hypothesize, may have also moved the isotopic ratios along the mixing line in Fig. 3.

Groundwater pumping may have recently drawn young water into the upper aquifer at the Munshiganj site, where irrigation pumping largely controls groundwater flow during

the dry season. Bangladesh is self-sufficient in food supply largely because irrigated dry-season crops are grown in addition to the traditional crops after the monsoon. During the irrigation season, January through March 2002, the average water table elevation dropped 2.3 cm/day (interpolated from the 45 monitoring wells in the 16-km² area around the sampling-well cluster; Fig. 4A). The drawdown calculated from the pumping rates of the 38 irrigation wells was similar: 4.9 cm/day if applied over only the 20% of land irrigated, and 1.2 cm/day when distributed over the entire area (18). These pumping-driven downward velocities imply plug-flow travel times to 30 m of 6.8 and 28 years, respectively. Thus, young carbon could be quickly transported to depth. Before the advent of irrigation pumping (~ 25 years ago), flow to depths of 30 m was extremely slow, limited by the negligible natural (i.e., without pumping) hydraulic gradients in the flat topography. Very little groundwater flow occurs during flooding (June to November) because inundation erases hydraulic gradients and downward flow by compression of water is negligible.

Recharging water is composed of a mixture of carbon-rich surface water (which enters the aquifer during the dry season) and rainwater (which enters the aquifer from March until flooding begins in June). Comparison of rainfall, evaporation, and changes in groundwater storage at a nearby long-term monitoring site (Fig. 4B) indicate that surface water contributes ~ 0.3 m ($\sim 40\%$ of re-

charge) yearly, whereas precipitation (less evaporation) contributes ~0.5 m (~60%). The recent observation that water levels rose in May 2002 from the levels in April by ~1.25 m before the monsoon confirms that surface water bodies recharge the aquifer. Infiltrating surface water receives heavy loadings from the untreated waste of the ~17,600 inhabitants of the 16-km² area. Hence this water contains high concentrations of dissolved carbon, as would water that infiltrates from rice paddies and through organic-rich pond and river sediments.

The observed arsenic mobility appears related to recent inflow of carbon through either organic carbon-driven reduction or displacement by carbonate. The distinctly older radiocarbon ages of DOC relative to DIC and methane imply that mobilization is not driven by detrital organic carbon. Water budgets indicate that the advent of massive irrigation pumping has drawn relatively young water into the aquifer over the last several decades, as may be typical of Bangladesh (19). Thus, irrigation pumping may affect arsenic concentrations, but not by the oxidation of sulfides as has been proposed. The low arsenic concentrations from the deeper aquifer indicate that deep wells may provide a source of clean water, an option that is already being implemented on an ad hoc basis (20). However, the apparent relation of arsenic mobility to inflow of organic carbon raises concerns about the appropriate depth of new drinking-water wells and their position relative to irrigation wells.

References and Notes

1. D. G. Kinniburgh, P. L. Smedley, Eds., *Arsenic Contamination of Groundwater in Bangladesh* (British Geological Survey Report WC/00/19, 2001) (www.bgs.ac.uk/arsenic/Bangladesh).
2. A. H. Smith, E. O. Lingas, M. Rahman, *Bull. WHO* **78**, 1093 (2000).
3. C. F. Harvey, *Environ. Sci.* **8**, 491 (2001).
4. R. Nickson et al., *Nature* **395**, 338 (1998).
5. P. L. Smedley, D. G. Kinniburgh, *Appl. Geochem.* **17**, 517 (2002).
6. T. R. Chowdhury et al., *Nature* **401**, 545 (1999).
7. D. Das et al., Bore-hole soil-sediment analysis of some As affected areas, in *Proc. Int. Conf. on Arsenic in Groundwater: Cause, Effect and Remedy*, Calcutta, December 1995.
8. See supporting data on Science Online.
9. F. H. Khan, *Geology of Bangladesh* (University Press, Dhaka, Bangladesh, 1991).
10. J. M. McArthur et al., *Water Resour. Res.* **37**, 109 (2001).
11. N. E. Keon et al., *Environ. Sci. Technol.* **35**, 2778 (2001).
12. D. B. Senn, H. F. Hemond, *Science* **296**, 2373 (2002).
13. C. A. J. Appelo et al., *Environ. Sci. Technol.* **36**, 3096 (2002).
14. D. K. Nordstrom, in *Minor Elements 2000: Processing and Environmental Aspects of As, Sb, Se, Te, and Bi*, C. Young, Ed. (Society for Mining, Metallurgy, and Exploration, Littleton, CO, 2000), pp. 21–30.
15. S. L. Goodbred Jr., S. A. Kuehl, *Geology* **27**, 559 (1999).
16. C. J. Yapp, H. Poets, *Geochim. Cosmochim. Acta* **50**, 1213 (1986).
17. M. J. Whitar, *Chem. Geol.* **161**, 291 (1999).
18. No rivers flow from the area during the dry season, so

pumped groundwater that is not evaporated or transferred into rice fields or ponds must re-infiltrate back into the aquifer. Thus, the drawdown (the net change in aquifer storage) during this period is controlled by the rate of evapotranspiration and transfer of groundwater with rice fields and ponds. The drawdown due to evapotranspiration, estimated by applying the Penman-Monteith equation to local meteorological data collected by the Bangladesh Water Development Board, is consistent with this water budget, increasing from 1.1 cm/day in January to 2.2 cm/day in March. Although no regional gradient is evident from the measured hydraulic heads, strong lateral flows controlled by the position of irrigation wells and recharge areas may create complex pathways for invading water. Applying Darcy's law to interpolated hydraulic heads and hydraulic conductivity es-

imated from pump tests gives an average lateral component to groundwater velocity of 1.7 cm/day, similar to the vertical component.

19. C. F. Harvey, *Science* **296**, 1563 (2002).
20. W. H. Yu, C. M. Harvey, C. F. Harvey, *Water Resour. Res.*, in press.
21. Supported by NSF grant EAR-0001098, NSF graduate fellowships, a grant from the Alliance for Global Sustainability, and National Institute of Environmental Health Sciences grant P30ES02109.

Supporting Online Material

www.sciencemag.org/cgi/content/full/298/5598/1602/DC1

Materials and Methods
References

5 August 2002; accepted 21 October 2002

Grasping Primate Origins

Jonathan I. Bloch* and Doug M. Boyer

The evolutionary history that led to Eocene-and-later primates of modern aspect (Euprimates) has been uncertain. We describe a skeleton of Paleocene plesiadapiform *Carpolestes simpsoni* that includes most of the skull and many postcranial bones. Phylogenetic analyses indicate that Carpolestidae are closely related to Euprimates. *C. simpsoni* had long fingers and an opposable hallux with a nail. It lacked orbital convergence and an ankle specialized for leaping. We infer that the ancestor of Euprimates was primitively an arboreal grasper adapted for terminal branch feeding rather than a specialized leaper or visually directed predator.

Extant primates are distinct from other eutherian mammals in having large brains, enhanced vision brought about in part by optical conver-

gence, the ability to leap, nails on at least the first toes, and grasping hands and feet (1, 2). Several adaptive scenarios have been proposed to explain these specializations: (i) "grasp-leaping" locomotion (3), which predicts simultaneous evolution of grasping and leaping; (ii) visually directed predation (4), which predicts simultaneous evolution of forward-facing orbits

Museum of Paleontology, University of Michigan, 1109 Geddes Road, Ann Arbor, MI 48109-1079, USA.
*To whom correspondence should be addressed. E-mail: carpo@umich.edu

Fig. 1. Hypothesis of phylogenetic relationships among select archontans, illustrating phylogenetic position of Carpolestidae based on cladistic analysis of 65 postcranial characters (25). Many fossil archontans were excluded from the analysis because postcranial skeletons for these groups have not yet been described. Cladistic analysis yielded a single most-parsimonious cladogram generated by an exhaustive search algorithm and rooted with *Asioryctes*: tree length = 117, consistency index = 0.75, retention index = 0.67. All characters were unordered. As for previous cladistic analyses (10), the topology supports a plesiadapiform-euprimate link, whereas the cladogram based on postcranial data presented here specifically allies Carpolestidae with Euprimates (Omomyidae plus Adapidae). Unambiguous synapomorphies supporting a carpolestid-euprimate link include morphology of distal humerus (character 10), a nail on the hallux (character 21), a sellar joint between metatarsal I and the entocuneiform (character 50), and lateral torsion of the distal metatarsal I (character 65).

